International Journal of Concrete Structures and Materials

RESEARCH Open Access

Thermal Cracking in High Volume of Fly Ash and GGBFS Concrete

Yingda Zhang[1,2*]

Abstract

Supplementary cementitious materials (SCMs) such as fly ash and ground granulated blast furnace slag (GGBFS) are found to control the maximum temperature and the accompanying thermal gradients effectively. However, SCMs also lead to low early age strength development. Thus, it is crucial to understand the cracking behaviour of SCMs-based concrete affected by the mix design parameters. In this paper, the thermal cracking resistance was evaluated using a rigid cracking frame (RCF) with a computer-controlled temperature profile. The temperature profile was determined using the software ConcreteWorks by assuming the centre point of the mass concrete. The free shrinkage frame (FSF) and match-curing oven follow the same temperature profile as RCF to measure the free total deformation and time-dependent mechanical properties of concrete, respectively. An analytical model was proposed to calculate the autogenous shrinkage and the thermal stress separately. A time-dependent cracking risk coefficient allowing to estimate the risk of early age cracking of concrete was also proposed.

Keywords Thermal cracking, Concrete, Rigid cracking frame, Fly ash, GGBFS, Model

1 Introduction

Due to restraint stresses caused by volume changes, the risk of early age cracking is exceptionally high in concrete structures such as dams, larger bridge piers, retaining walls, and foundations. The early age of total deformation contributes to different deformation components, including autogenous shrinkage, drying shrinkage and thermal effects (contraction or expansion). When the total deformation is restrained, it leads to a significant tensile stress development which may cause cracking if it exceeds the tensile strength of concrete.

According to ACI207.1R-05 (2012), the combined effect of heat produced by the cement hydration and relatively poor heat dissipation conditions leads to a considerable rise in temperature within a few days after mass concrete placement. As the cement hydration continues, the heat generated increases the internal temperature of concrete and produces differential thermal gradients between the internal and the surface of concrete structures because of the low thermal conductivity of concrete (Zhu, 2014). The thermal gradients produce tensile stress near the surface, leading to surface cracking. Meanwhile, the interior of the structure is subjected to compressive stress. When the ambient temperature drops, the interior will be subjected to tensile stress resulting from thermal gradients and external restraint.

Tensile stress caused by restrained autogenous shrinkage is critical in early age mass concrete. Autogenous shrinkage is the time-dependent reduction in the volume of concrete due to the internal consumption of moisture due to the hydration process. Self-desiccation is the driving force and one of the primary underlying mechanisms of autogenous shrinkage (Kovler & Zhutovsky, 2006).

Journal information: ISSN 1976-0485 / eISSN 2234-1315.

*Correspondence:
Yingda Zhang
yingda.zhang@mail.xhu.edu.cn
[1] School of Architecture and Civil Engineering, Xihua University, Chengdu 610039, China
[2] Centre for Infrastructure Engineering and Safety, School of Civil and Environmental Engineering, The University of New South Wales, Sydney, NSW 2052, Australia

Autogenous shrinkage is considered as a fundamental component of shrinkage because the volume reduction of concrete occurs without loss of moisture to the environment. According to (Neville & Aitcin, 1998), autogenous shrinkage is relatively low in normal strength concrete with w/b exceeding 0.42. However, in high strength concrete, autogenous shrinkage increases and can be the same amount as drying shrinkage.

Drying shrinkage is critical in concrete elements with large surface area-to-volume ratios, such as pavements, overlays, and bridge decks. It happens when the physical loss of moisture from concrete to the environment. In unsealed concrete surfaces, the evaporation rate of moisture is dependent on environmental factors, including wind, relative humidity, solar radiation and ambient temperature (Bissonnette, et al., 1999; Hansen & Almndaiheem, 1987; Truman, et al., 1991). Compared to thermal and autogenous shrinkage, mass concrete structures susceptible to drying shrinkage are less significant within a few days after casting concrete. To some extent, proper curing is essential to minimise the impacts of restrained drying shrinkage.

The early age tensile stress depends not only on the early age deformation, as mentioned above, but also on the development of mechanical properties such as tensile strength, elastic modulus, and viscoelastic properties such as stress relaxation due to tensile creep. The previous research (Springenschmid & Breitenbücher, 1998) reported that the elastic modulus of concrete develops very fast in the first 24–36 h after placement. Many studies have shown that the gain in elastic modulus is faster than that of tensile strength during this time (De Schutter & Taerwe, 1996; Gutsch, 2002), which means the development of tensile stress is high. The viscoelastic behaviour such as stress relaxation due to tensile creep is also significant in contributing to the early age of stress development in concrete. It has been reported that the tensile creep releases 50–60% of the stress than that stress developed without relaxation (Altoubat & Lange, 2001; Gutsch, 2002; Tao & Weizu, 2006; Zhang, et al., 2021). However, the above discussion resulted from the investigation of the mechanical properties under either standard curing or ambient curing conditions. Therefore, evaluating the development of mechanical properties under the same temperature history as the mass concrete structures should be considered.

Numerous researchers have investigated ways to mitigate the risk of early age thermal cracking. (Batog & Giergiczny, 2017) reported that reducing the amount of heat released is mainly achieved through changes in mix design parameters such as w/b ratio, cement content and use of supplementary cementitious materials (SCMs), including fly ash and ground granulated blast furnace slag (GGBFS). (Ballim & Graham, 2009) showed that the increasing amount of fly ash or GGBFS in the cement composition decreased the rate and amount of heat produced. (Mehta & Monteiro, 2006) revealed that replacing ASTM Type I cement with Type II or Type IV cement, and pozzolans partially substituting Portland cement significantly decreased the adiabatic temperature in concrete. They also stated that the increasing w/b ratio reduces the heat of hydration and slows down the heat kinetics at an early age of hydration. (ACI207.2R-07, 2007) suggested alternative curing methods to reduce the heat produced by cement hydration, which reduces the risk of early age thermal cracking. (Gołaszewski, et al., 2023) examined the engineering properties of self-compacting concrete with fly ash and slag. They found that fly ash exhibited the best performance in enhancing the thermal and shrinkage properties of concrete, while slag concrete was the most effective considering the strength and maintaining the thermal and shrinkage properties. (Cai et al., 2022) investigated the long-term shrinkage performance of concrete under large temperature differences. They found the cyclic temperature differences caused accumulation of maximum restrained stress in concrete. Coat curing showed the best performance in resisting cracking. (Eisa et al., 2022) explored the drying shrinkage and thermal expansion properties of biaxial geogrid reinforced geopolymer concrete. They also found that biaxial geogrid reinforcement in geopolymer concrete led to a reduction in drying shrinkage and thermal expansion strains. However, for some of the above studies, such as (Batog & Giergiczny, 2017), there is no restrained thermal cracking test or thermal stress test, so it is difficult to determine if their mixtures crack.

A lot of effort has been directed at devising test methods to determine restraint stresses. Conventionally, the two most common test methods, such as rigid cracking frame (RCF) (Breitenbucher, 1990) and temperature stress testing machine (TSTM) (Springenschmid et al., 1985), are used to determine the restraint stress at an early age. Test methods such as the RCF can provide the measure of thermal stress considering various factors such as thermal strain, elastic modulus, degree of restraint and stress relaxation (Breitenbucher, 1990). According to (Mangold, 1998), the RCF provides a 100% degree of restraint for fresh concrete and approximately 80% for hardened concrete. On the other hand, the TSTM achieves 100% restraint by compensating for any length change in the specimen by adjusting a movable crosshead with a computer-controlled system (Springenschmid et al., 1985). TSTM can completely suppress the deformation against the combined effects of thermal strain and autogenous shrinkage. However, it is unlikely that full restraint will be encountered in most common

situations. Therefore, this paper adopted the RCF test because it can fully reproduce in situ restraint stress in the laboratory in accordance with (Whigham, 2005).

This paper intends to investigate the tensile stress development and cracking for three concrete mixes with SCMs such as fly ash and GGBFS using RCF. Secondly, this study is committed to developing an analytical model to calculate the autogenous shrinkage and thermal contraction-induced stress separately, allowing for avoiding experimentations related to RCF which are not straightforward tests. This research can also contribute to developing a performance-based specification to examine the risk of early age concrete cracking due to restrained shrinkage and temperature variation.

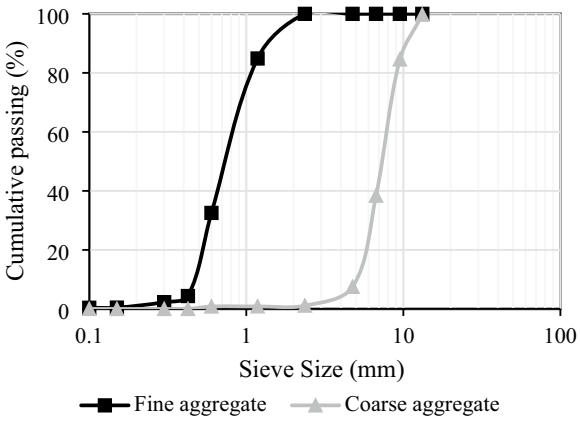

Fig. 1 Particle size distribution of coarse and fine aggregates

2 Experimental Programme

2.1 Materials and Mix Proportion

The concrete mixes were produced with general purpose (GP) cement, fly ash and GGBFS. Table 1 summarises the chemical composition of the GP cement, fly ash and GGBFS by X-ray fluorescence (XRF) analysis according to (AS, 2564–1982, 1982). The coarse aggregate is basalt with a maximum nominal size of 10 mm, and local Sydney sand with a maximum nominal size of 2.36 mm is used as fine aggregate. The coefficient of thermal expansion (CTE) of basalt is determined as 6.8×10^{-6} °C. The water absorption and specific gravities are 1.08% and 2.8 for coarse aggregate and 3.5% and 2.65 for fine aggregate, respectively. The particle size distribution (PSD) for coarse and fine aggregates is shown in Fig. 1.

Three concrete mixes were prepared to investigate the effect of fly ash and GGBFS on the concrete properties, including the time-dependent mechanical properties, autogenous shrinkage development, thermal stress and the risk of early age cracking potential. 'N50' was designated for the concrete mixes because the nominated compressive strength for all mixes was 50 MPa. Mixture '0' was the reference concrete mixes without fly ash or GGBFS. Fly ash and GGBFS replace 30% and 60% of GP cement by weight because 30% fly ash and 60% are practical and widely used in Australian industry. Hence, 'FA30' and 'G60' were designated for fly ash and GGBFS concretes. Initially, the water-to-binder ratio of concrete mixes with fly ash and GGBFS was consistent with reference concrete. However, the compressive strength of fly ash and GGBFS concrete was significantly lower than that of the control mix. As such, the water-to-binder ratio of concrete with fly ash and GGBFS was reduced to achieve the targeted compressive strength. Moreover, a competitive market superplasticiser was utilised to improve the workability of the concrete mixes. The mix design proportions are presented in Table 2.

Table 1 Chemical composition of GP cement, fly ash and GGBFS

Chemical composition	GP cement (wt.%)	Fly ash (wt.%)	GGBFS (wt.%)
SiO_2	18.8	65.9	34.1
Al_2O_3	5	22.1	15.4
Fe_2O_3	2.8	3.4	0.8
CaO	63.8	1.6	36
MgO	1	0.7	6.6
Na_2O	0.3	0.6	0.4
K_2O	0.7	1.8	0.6
TiO_2	0.3	0.9	2.4
SO_3	3	0.1	2.5
Mn_3O_4	–	0.1	1.1

2.2 Temperature Profile Simulation

Since the temperature profile of mass concrete is difficult to obtain, the temperature profile was simulated using the software ConcreteWorks. ConcreteWorks has been developed to predict the temperature profile of mass concrete. ConcreteWorks provides the concrete temperature history of each concrete mixture based on the geometry of the element, mix design proportions, chemical composition of the cementitious materials, thermal coefficient of expansion of aggregates, and the environmental effects. In this study, the member type in ConcreteWorks was selected as mass concrete with rectangular columns. The dimension of width and depth were 1 m and 1.5 m, respectively. The minimum and maximum temperature was input as 22–23 °C according to the laboratory environmental conditions. The input number of days was 4 days (96 h). The input project location was selected as Port Arthur because the default location system in ConcreteWorks is US city and Port Arthur is a representative costal city,

Table 2 Mix proportions of concrete

Sample ID	Mix proportions by weight (kg/m^3)					w/b ratio
	GP Cement	FA	GGBFS	Coarse Agg	Fine Agg	
N50-0	510	0	0	927	759	0.4
N50-FA30	355	155	0	955	782	0.3
N50-G60	205	0	305	941	770	0.35

similar to Sydney. The type of fly ash was selected as Class F. Then the temperature profile can be obtained by ConcreteWorks. The simulated temperature profile was applied to the RCF, FSF and match-curing oven. In addition, the temperature profile was assumed at the centre point of the mass concrete element. It should be noted that ConcreteWorks considers the mixture designs assuming the statistically representative properties of Portland cement, fly ash and GGBFS, it cannot specifically consider the effect of fly ash and GGBFS used in this particular study. The effects of fly ash and GGBFS on heat generation and hydration may significantly vary depending on their chemical compositions of them. Fortunately, the results of temperature profile simulated by ConcreteWorks have been successfully used and validated in previous research (Byard et al., 2010; Sargam et al., 2019; Tankasala et al., 2017). As a result, this study assumed that the simulated profile was reasonably correct.

2.3 Mechanical and Fresh Properties Test

Mechanical properties of concrete, including the compressive strength, tensile strength and elastic modulus, were tested at the ages of 1, 3, 7, and 28 days based on the Australian Standard (AS1012.9–2014, 2014), (AS, 1012.10–2000, 2000) and (AS, 1012.17–1997, 1997), respectively. Note that the 1- and 3-day cylinders were cured in a match-curing oven, while the 7- and 28-day cylinders were moved to a standard curing condition (the temperature at 23 ± 2 °C and relative humidity of 95 ± 5%) after the RCF specimen had cracked (≈ 5 days). The dimension of the cylindrical specimen was 100 mm in diameter by 200 mm in height. The slump test evaluates the workability of concrete in accordance with (AS, 1012.3.1–2014, 2014). The air content of concrete was tested according to (AS, 1012.4.2–2014, 2014). The fresh density of concrete was obtained by weighing the concrete during pouring according to (AS, 1012.5–2014, 2014), which could eliminate the influence of hydration reaction.

2.4 Match-Curing Oven

Fig 2 presents the match-curing oven used to cure the concrete cylinders. To determine the development of mechanical properties of concrete placed in the RCF, tested cylinders are cured under the same temperature profile as the specimen in the RCF and FSF. As mentioned in the previous section, the match-curing oven was used to test the mechanical properties of concrete at the age of 1 and 3 days. The relative humidity in the match-curing oven was controlled at 95 ± 5% to avoid any moisture loss.

2.5 Rigid Cracking Frame (RCF) Test

Due to the complex interaction of different factors such as thermal strain, elastic modulus, degree of restraint, and stress relaxation, traditional methods solely based on the measurement of concrete deformation (e.g.

Fig. 2 Match-curing oven

restrained ring test) cannot determine the thermal and other restraining stresses in young hardening concrete. The RCF test can give a measurement of thermal stress by inherently considering the influence of elastic modulus, autogenous shrinkage, tensile creep, etc. The RCF is made up of a concrete specimen held by two mild steel crossheads, which are fixed in place by two Invar sidebars, the dimension of the RCF cross-section is 150×150 mm, as shown in Fig. 3.

For the rigid sidebars to provide the proper restraint, the concrete specimen must be fixed at both ends. Therefore, the steel crossheads are constructed in such a way that they contain dovetails lined with teeth for gripping concrete. Crosshead braces are bolted to the top and bottom of each crosshead to prevent the slip of the concrete sample, and these restrain expansion as the concrete goes into tension. Since the midsection of the concrete sample in RCF test has a narrower width than the crosshead section. This concentrates the stress in the test area, so that cracks and most of the strain occur in midsection. The RCF is made with a thermally insulated formwork that enables measurements to begin immediately after fresh concrete has been placed and helps control the temperature of the sample.

To minimise the effect of temperature change on the length of the side bars, Invar steel is used to make the sidebars. Each bar was fitted with strain gauges capable of measuring the small axial strains produced by the combined effects of thermal and autogenous shrinkage in the concrete. In the central portion of the specimen, the stresses were uniaxial, and hence, a uniform stress distribution was assumed. The measured strains in the Invar sidebars could thus be used to compute the corresponding stress development in the restrained concrete specimen. The RCF test was set to follow the temperature profile simulated by ConcreteWorks within the first 96 h. If the specimen is not cracked during the test period, then it undergoes an artificially cooling process. In other words, the operator manually operates the computer to control the water circulator of the RCF, driving the RCF to cool down at a rate of 1 °C/hour to accelerate the development of tensile stress and induce thermal cracking. The temperature and stress of the specimen were continuously monitored until the specimen was cracked.

2.6 Free Shrinkage Frame (FSF) Test

The FSF test was used to evaluate the free total deformation including thermal and autogenous shrinkage. As shown in Fig. 4, the FSF is the framework that is thermally controlled by copper tubing and a supporting Invar steel frame. Thus, the fresh concrete used in this study was allowed to be placed in FSF to cure at the

Fig. 3 Test of rigid cracking frame

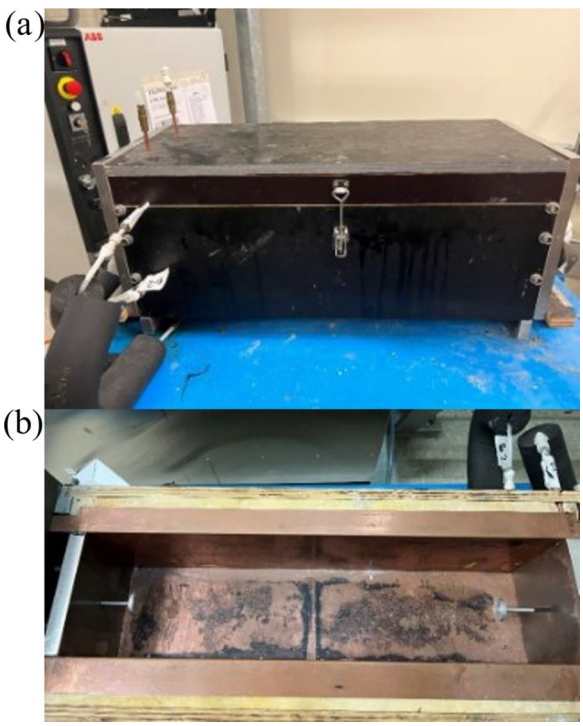

Fig. 4 Test of free shrinkage frame: **a** actual frame; **b** inside of the frame

same temperature profile as RCF. Two end steel plates measured the free total deformation with an Invar rod to a linear variable displacement transducer (LVDT). The dimension of the FSF was 150×150×600 mm. The FSF maintained the specimen under a sealed condition so that neither moisture loss during the test nor, thus, drying shrinkage occurred in the FSF test.

2.7 Autogenous Shrinkage Test

As mentioned in Sect. 2.6, the FSF allows for measuring the total deformation including both autogenous shrinkage and thermal deformation (expansion and contraction). But these two deformations cannot be assessed separately using this test. Therefore, this section aims to assess the autogenous shrinkage using standard concrete prisms. The tests were carried out at the constant temperature of 23 °C. It should be noted that the autogenous shrinkage measured using concrete prisms at 23°C will not be identical to the autogenous shrinkage of mass concrete because of the difference in temperature, dimension and hydration degree. The increase in concrete autogenous shrinkage due to the increase in temperature was not accounted for in this study. As a result, the thermal deformation can be deduced from the difference between total deformation measured using the FSF and autogenous shrinkage measured using the standard concrete prisms. The autogenous shrinkage specimen is shown in Fig. 5. The size of the standard shrinkage prisms in Australia is 280×75×75 mm (AS1012.8.4–2015, 2015). After demoulding, all faces of autogenous shrinkage specimens were well-wrapped using a self-adhesive water-proof aluminium foil to avoid any moisture loss to the environment (Gibert et al., 2017). Measurements were carried out once a day for 5 days (120 h).

Fig. 5 Autogenous shrinkage specimens

3 Test Results and Discussion

3.1 Temperature Profile

Fig 6 shows the temperature profile data obtained from ConcreteWorks. The peak temperature of the control mixture was higher than those of fly ash and GGBFS mixtures. The time for the maximum temperature was also delayed when the addition of fly ash and GGBFS. The peak temperature for the control mixture was 64.2 °C, and it occurred at 20 h after pouring concrete, which was higher and earlier than 51.4 °C, 26 h for FA30 concrete and 49.4 °C, 28 h for G60 concrete, respectively, which indicates that the fly ash and GGBFS could effectively reduce the heat of hydration and resultant thermal cracking in concrete structures.

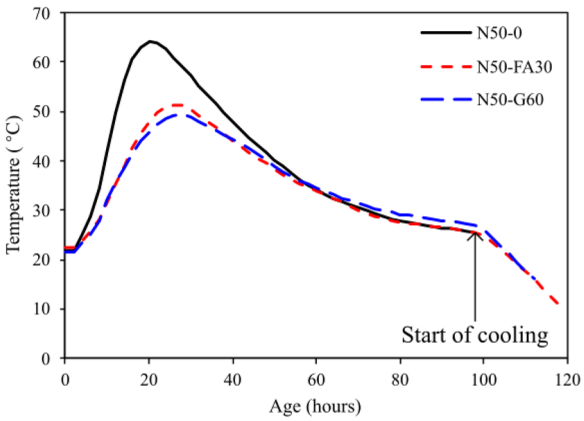

Fig. 6 Simulated temperature profile of concrete

3.2 Mechanical and Fresh Properties of Concrete

Tables 3 and 4 show the mechanical properties of concrete, including the compressive strength, splitting tensile strength, elastic modulus and fresh properties such as slump, air content and fresh density for each concrete mix. It can be seen that the incorporation of fly ash and GGBFS decreased the compressive strength, tensile strength and elastic modulus compared to that of reference concrete, especially at an early age. This is attributed to the low activity of fly ash and GGBFS, which slows down the hydration process (Wang et al., 2015).

Table 3 Mechanical properties of concrete

Sample ID	Compressive strength (MPa)				Splitting tensile strength (MPa)				Elastic modulus (GPa)			
	1d	3d	7d	28d	1d	3d	7d	28d	1d	3d	7d	28d
N50-0	25.5	36.3	43.6	56.9	2.7	3.7	4	4.6	31.2	36.8	37.8	39
N50-FA30	20.3	33.7	42.6	55.2	2.2	3.1	3.9	4.5	24.3	28.7	33.2	37
N50-G60	22.1	35.9	43.1	55.4	2.2	3.6	3.8	4.4	22.6	25.2	31.2	33.2

Table 4 Fresh properties of concrete

Sample ID	Slump (mm)	Air content (%)	Density (kg/m^3)
N50-0	75	2.5	2441
N50-FA30	30	4.8	2383
N50-G60	65	4	2445

3.3 Rigid Cracking Frame and Free Shrinkage Frame Results

Fig 7 presents the stress development obtained from the RCF test and the free deformation development of reference and SCM concretes. It can be seen that all three mixtures exhibited swelling behaviour at a very early age. Previous studies also reported this phenomenon (Igarashi et al., 2000; Markandeya et al., 2018; Wei & Hansen, 2013). This could be attributed to thermal dilation due to the heat of hydration, absorption of bleeding water, water adsorption by filler, CH growth and primary ettringite formation (Bjøntegaard et al., 2004; Carette et al., 2018; Craeye et al., 2010). Reference concrete had the highest swelling deformation, which was also attributed to the higher temperature rise shown in Fig. 6 in addition to the possible reasons mentioned above. This also explained the highest compressive stress development for the reference concrete as determined by the RCF test (see Fig. 7a). In other words, under the restrained condition, the higher expansion of the reference mixture corresponded to a higher initial precompression. According to Wei and Hansen (Wei & Hansen, 2013), the strain for free shrinkage frame at the zero-stress temperature (T_{zs}) (see Fig. 7a) is called zero-stress strain (ε_{zs}), and it is referred to as the starting point of contraction for comparison (see Fig. 7b). Note that the ε_{zs} is not necessarily zero because the compressive stress of young concrete is relaxed. Thus, by setting the value of ε_{zs} is numerically equal to zero, then the increase of free deformation after ε_{zs} is denoted as "absolute free total contraction" (see Fig. 7c). As such, the absolute free total contractions were compared for assessing the cracking risk.

Fig 7c shows the measured stress and absolute free total contraction of three concrete mixes. The absolute free total contraction of the control mixture was 295 με at 96 h, which was higher than that of N50-F30 and N50-G60 concretes with 160 and 241 με, respectively. After 96 h, the artificial cool process produced a high rate of contraction development. When the fly ash and GGBFS were incorporated into the concrete mixes, the significant reduction of the absolute free total deformation resulted in reduced tensile stress development This will be discussed in Sect. 3.5.

3.4 Autogenous Shrinkage of Concrete

Fig 8 presents the mean value of the experimentally measured autogenous shrinkage for each concrete mixture. The measurement of autogenous shrinkage started 24 h after casting. The absolute value of autogenous shrinkage strain at 5 days (120 h) was 90 με, 56 με and 102 με, which decreased by 38% and increased by 13% for concrete mixes from 0% SCM to 30% fly ash and 60% GGBFS, respectively. Similar results can be found in (Gao et al., 2013; Lee et al., 2006). (Gao et al., 2013) demonstrated that the autogenous shrinkage for concrete mixes with 30% fly ash was approximately 30% lower than reference concrete at an early age. The results can be explained by fly ash as a filling powder material that does not take part in early hydration. Hence, the autogenous shrinkage is effectively decreased (Gao et al., 2013). (Lee et al., 2006) showed that the early age of autogenous shrinkage increased with GGBFS content. This is attributed to the incorporation of GGBFS leads to a finer pore structure, contributing to lower relative humidity, thus increasing the self-desiccation and autogenous shrinkage. The underlying logic of conducting the autogenous shrinkage test is that the absolute free deformation measured from FSF consists of thermal strain and autogenous

(See figure on next page.)

Fig. 7 Measured stress of concrete from RCF test and strains of concrete from FSF test: **a** temperature and stress; **b** stress and free total deformation; **c** stress and absolute free total contraction

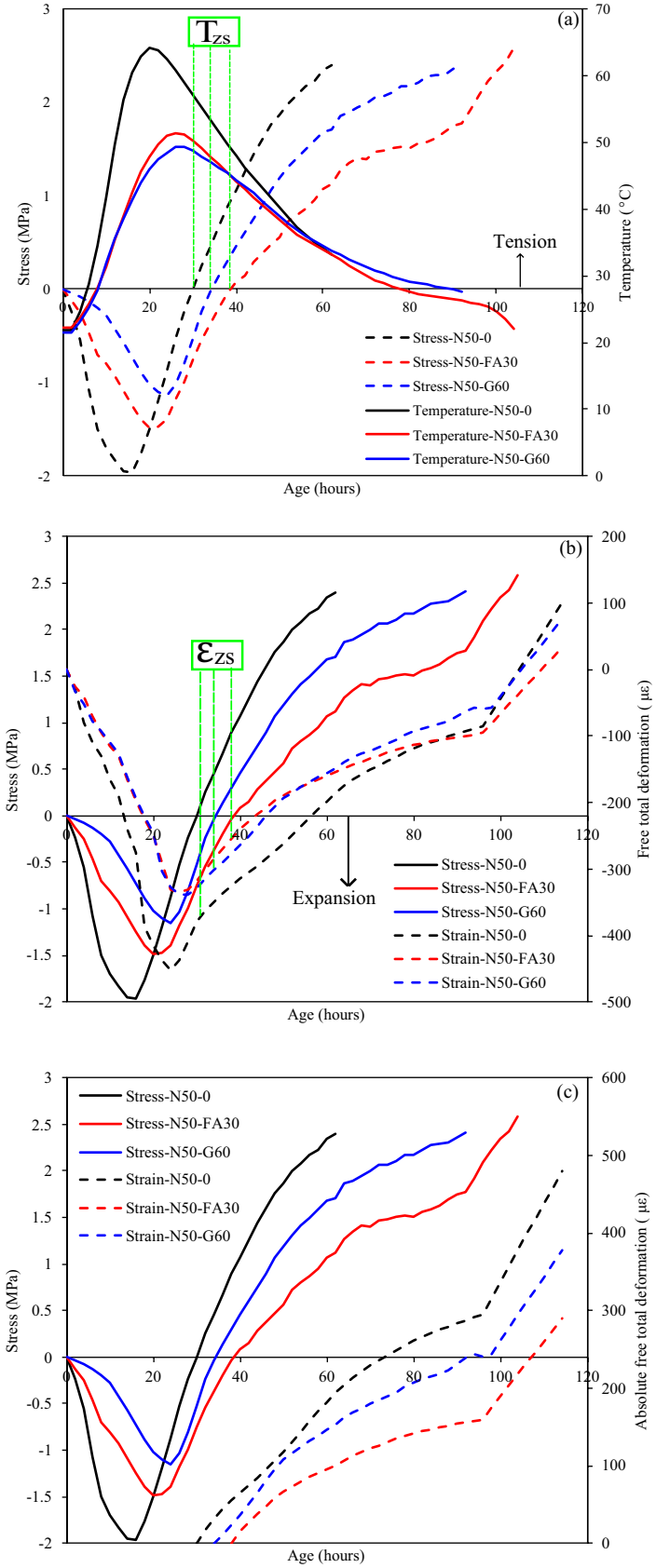

Fig. 7 (See legend on previous page.)

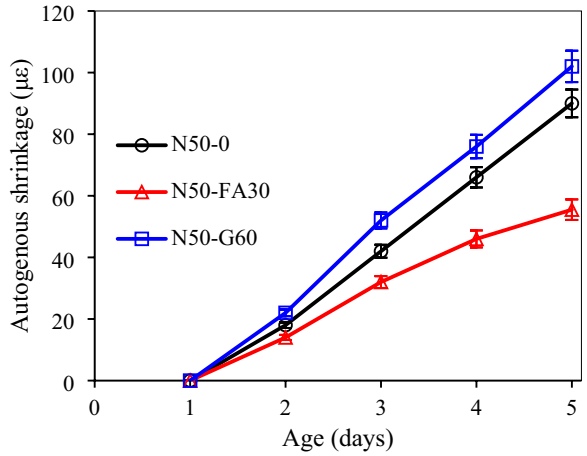

Fig. 8 Measured autogenous shrinkage of concrete from prism test

shrinkage. After measuring autogenous shrinkage, the thermal strain can be simply deduced. Then the autogenous shrinkage-induced stress and thermal stress can be calculated separately. This will be discussed in Sect. 4.

3.5 Tensile Stress Development

The behaviour of concrete in the RCF can be described in five stages (Breitenbucher, 1990). The RCF test results of stress development for all concrete mixtures are presented in Fig. 9. The concrete specimen cracked at 62 h for the control mixture, and the cracking stress was 2.4 MPa. The cracking stress can be calculated using the product of the Invar strain and its elastic modulus. However, N50-FA30 did not fail in the first 96 h. It cracked after 8 h of artificial cooling, which indicated the decreased cracking potential of the mixture, while for the GGBFS mixture the cracking time was 92 h which was also significantly delayed compared to that of the reference mixture. In view of these results, the addition of SCMs lowered the early age cracking risk. This was attributed to the significant reduction in the free total deformation that will be discussed in Sect. 3.4 and Fig. 8 and the elastic modulus development (Table 3). Secondly, as shown in Fig. 6, the temperature rise decreased compared to that of the control mixture. Fly ash was more effective in reducing the cracking risk than GGBFS because the absolute free total contraction of GGBFS was higher than that of fly ash mixture as mentioned in Sect. 3.3. Although the tensile strength of SCMs concrete decreased, the combined effect of temperature rises and elastic modulus compensated for the negative impact of tensile strength, resulting in an overall enhancement in performance of resistance to cracking.

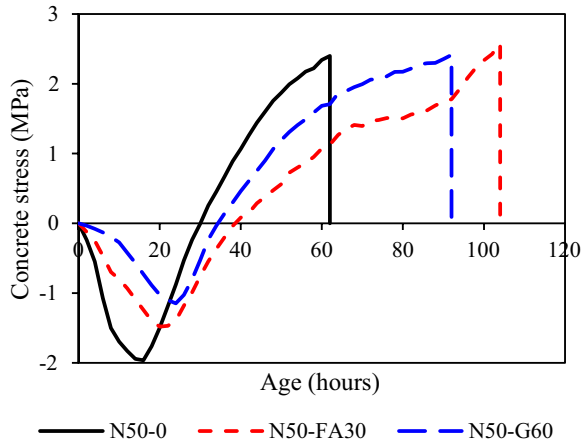

Fig. 9 Comparison of thermal stress development of different concrete mixes

Table 5 summarises the time and temperature at a zero-stress state and the time and temperature at cracking. The incorporation of fly ash and GGBFS reduced the zero-stress temperature and the zero-stress time because of the lower peak temperature in the applied temperature profile. The addition of SCMs also decreased the cracking temperature and delays the time to cracking, and the lower cracking temperature indicated the better resistance to early age cracking of the mixes. This is attributed to the decreased rate of temperature development and elastic modulus development (Byard et al., 2010). Moreover, (Wei & Hansen, 2013) reported that the replacement of cement by GGBFS can effectively resist concrete cracking. (Markandeya et al., 2018) conducted the RCF tests using different types of GGBFS with the same percentage of replacement. They found that the temperature risk and cracking potential decreased compared to that of the control mixture regardless of the slag types. (Riding et al., 2008) reported that the introduction of fly ash in concrete delayed the tensile stress development, leading to a low-level tendency to crack. Therefore, the results that concrete cracking time is delayed with an increasing proportion of fly ash or GGBFS in this research are rational.

Table 5 Cracking indices from RCF tests

Mix	Zero stress		Cracking	
	Time (h)	Temperature (°C)	Time (h)	Temperature (°C)
N50-0	30	57.2	62	33.2
N50-FA30	38	45.5	104	19.3
N50-G60	34	47.0	92	27.5

4 Analytical Modelling for Tensile Stress Development in RCF

4.1 Analytical Solution for Tensile Stress Development

According to ACI 207.2 (ACI207.2R-07, 2007), the tensile stress due to restraint can be calculated using Eq. (1):

$$\sigma_t = D_R \varepsilon_t E_c, \tag{1}$$

where D_R is the degree of restraint which can be computed based on the rigidity of restraining element and concrete, as shown in Eq. (2); ε_t is the total contraction due to shrinkage and thermal deformation caused by heat dissipation; E_c is the elastic modulus of concrete.

$$D_R = \frac{1}{1 + \frac{A_c E_c}{A_I E_I}}, \tag{2}$$

where A_c is the cross-sectional area of concrete which is equal to 22500 mm^2 in the RCF test; A_s is the cross-section area of Invar side restraining bars in the RCF test, which is equal to 15710 mm^2; E_I is the elastic modulus of Invar side bar which is equal to 137 GPa.

As mentioned in the previous study of (Zhang et al., 2021, 2022), stress relaxation due to tensile creep is critical. Hence, in some existing codes, such as JCI guidelines (JCI, 2016), the effective elastic modulus method is utilised to take into account the creep effect (Maruyama & Lura, 2019). Although this approach captures the order of magnitude of stress relaxation that occurs in concrete, it might be a bit conservative because the creep increases more slowly under gradually increasing stress than under constant stress (Kovler, 1994). In this study, a reduced creep coefficient by implementing an ageing coefficient and age-adjusted effectively modulus method was adopted according to (Gilbert & Ranzi, 2011). Note that the ageing coefficient in age-adjusted effectively modulus method is less than 1.0 because a reduced creep coefficient can be used to calculate creep strain if stress is gradually applied. Also, the change of stress may be attributed to restraint to creep and shrinkage, or variations of temperature, or combinations of these. The expression of age-adjusted effective modulus is shown as follows:

$$\overline{E}_e = \frac{E_c}{1 + \chi(t,\tau)\varphi(t,\tau)}, \tag{3}$$

where $\varphi(t,\tau)$ is the tensile creep coefficient which can be obtained from the tensile creep model in Sect. 4.3; $\chi(t,\tau)$ is the ageing coefficient and the recommended value of the ageing coefficient is 0.80 for relaxation problems (Cheng et al., 2020; Gilbert & Ranzi, 2011).

Hence, the elastic modulus of concrete in Eqs. (1) and (2) should be changed to the age-adjusted effective modulus. The tensile stress and degree of restraint can be rewritten as shown in Eqs. (4) and (5):

$$\sigma_t = D_R \varepsilon_t \overline{E}_e, \tag{4}$$

$$D_R = \frac{1}{1 + \frac{A_c \overline{E}_e}{A_I E_I}}. \tag{5}$$

It should be noted that the above analytical models have been validated in a previous study using 21 independent sets of experimental data (Zhang, et al., 2021). The calculated degree of restraint varied from 1.0 to 0.72, 1.0 to 0.76 and 1.0 to 0.78 for control, fly ash and GGBFS concrete mixes, respectively. Similar results were obtained by (Slatnick et al., 2011). They stated that the degree of restraint was equal to 1 when the concrete is fresh and decreased to approximately 0.73 for hardened concrete. The total contraction of concrete in Eq. (4) is considered as the sum of the autogenous shrinkage and thermal contraction due to heat dissipation, as shown in Eq. (6):

$$\varepsilon_t = \varepsilon_{au} + \varepsilon_T, \tag{6}$$

where ε_{au} is the autogenous shrinkage measured from concrete prism; ε_T is the thermal contraction using the measured free deformation strain obtained from FSF minus the autogenous shrinkage or using the CTE multiples with temperature changes, as shown in Eq. (7):

$$\varepsilon_T = \alpha \Delta T. \tag{7}$$

By substituting Eqs. (5), (6) and (7) into Eq. (4), the total tensile stress of concrete can be expressed in terms of autogenous shrinkage induced stress and thermal stress, as shown in Eq. (8):

$$\sigma_t = \sigma_{au} + \sigma_T, \tag{8}$$

where σ_{au} and σ_T are the autogenous shrinkage induced stress and thermal stress, respectively, as shown in Eq. (9a) and (9b):

$$\sigma_{au} = \frac{\overline{E}_e \varepsilon_{au}}{1 + \frac{A_c \overline{E}_e}{A_I E_I}}, \tag{9a}$$

$$\sigma_T = \frac{\overline{E}_e \alpha \Delta T}{1 + \frac{A_c \overline{E}_e}{A_I E_I}}. \tag{9b}$$

The newly proposed analytical model from Eq. (9a) and Eq. (9b) can separate the autogenous shrinkage-induced stress and thermal stress. In this model, autogenous shrinkage of concrete can be simply measured on a prism test, elastic modulus can also be measured using a straightforward experimental test on concrete cylinders,

and the temperature variation can be determined through the software ConcreteWorks. The other required parameters such as coefficient of thermal expansion and tensile creep coefficient will be explained in Sect. 4.2 and Sect. 4.3, respectively.

4.2 Evaluation of Coefficient of Thermal Expansion (CTE)

As mentioned above, the CTE of concrete is one of the most important parameters for evaluating thermally induced strain and stress. Concrete with a high CTE is generally leading to a higher risk of cracking. According to Eq. (7), CTE can be rewritten using the thermal strain divided by the temperature change, as shown in Eq. (10):

$$\alpha = \frac{\varepsilon_T}{\Delta T}. \tag{10}$$

In Eq. (10), ε_T can be determined using the absolute free deformation from FSF minus the measured autogenous shrinkage from the prism, ΔT can be evaluated by calculating the temperature difference between two adjacent temperatures.

(Li et al., 2021) conducted a precise measurement of CTE of concrete at an early age using a newly built temperature stress testing machine (TSTM), stepped temperature profiles and temperature cycles ranging between 18 and 25 °C. They observed that the measured CTE showed a rising trend. The measured CTE increased from 7.2 to 12.3×10^{-6} °C for concrete with a w/b of 0.42. However, in the current research, the CTE values are quite fluctuated over time within the range between 5.8 and 12.0×10^{-6} °C, as shown in Fig. 10. This may be due to the difference between the TSTM test and the RCF test. Moreover, this study considered continuous temperature profiles based on the heat of hydration instead of stepped temperature profiles, which may affect the measured CTE values. As such, the CTE was calculated according to Eq. (10) and the average values were adopted, which were approximately equal to 8.5, 7.1 and 8.4×10^{-6} °C for OPC, fly ash and GGBFS concrete, respectively. Similar results can be found in (Gao et al., 2011; Shui et al., 2010). (Shui et al., 2010) illustrated that replacing the cement with fly ash and GGBFS lowers the CTE of the hardened cement paste. The reduction in CTE of fly ash and GGBFS systems is mainly due to the change in the porosity and portlandite (CH) (Shui et al., 2010). (Gao et al., 2011) also showed that the CTE of fly ash concrete is lower than reference concrete. Thus, the results that CTE of concrete decreased with an increasing proportion of fly ash or GGBFS in this research seems to be reasonable.

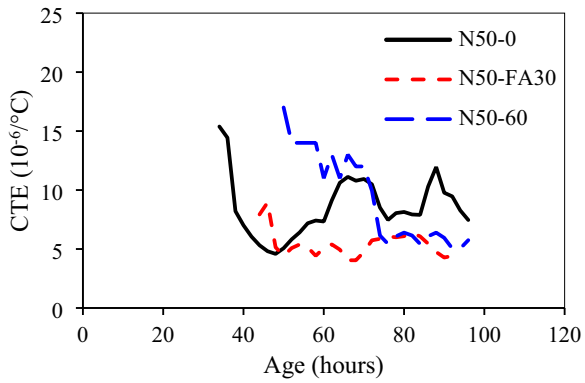

Fig. 10 Calculated coefficient of thermal expansion of different concrete mixes

4.3 Basic Tensile Creep Coefficient

It is critical to take into account the tensile creep of concrete into tensile stress development as it leads to stress relaxation. Most models such as (ACI209R, 2008) and (AS3600-, 2018, 2018) predominately apply compressive creep, and the drying and basic creep are not distinguished in these models. Instead, (FIB, 2010) is a commonly used code for predicting basic creep. It considers the effects of curing temperature and hydration degree on the creep coefficients by calculating the temperature-adjusted concrete age. However, according to (Dabarera et al., 2021), the basic tensile creep coefficient was underestimated by FIB, 2010 model. They also proposed a modified tensile creep model based on FIB, 2010 model and this model has been successfully validated by the results in (Atrushi, 2003; Ji et al., 2013). In this study, the experimental test conditions are similar to the test conditions conducted by (Dabarera et al., 2021). Therefore, the modified tensile creep model proposed by (Dabarera et al., 2021) is adopted for predicting the basic tensile creep coefficient $\varphi_{bc}(t,t_0)$ in this paper. The modified model is shown as follows (Dabarera et al., 2021):

$$\varphi_{bc}(t,t_0) = \beta_{bc}(f_{cm})\beta_{bc}(t,t_0), \tag{11}$$

where $\beta_{bc}(f_{cm})$ is the strength-dependent factor which is shown in Eq. (12a); $\beta_{bc}(t,t_0)$ is the time-development function which is shown in Eq. (12b):

$$\beta_{bc}(f_{cm}) = \frac{7}{(f_{cm28})^{0.7}}, \tag{12a}$$

$$\beta_{bc}(t,t_0) = \ln\left\{\left(\frac{55}{t_{0,adj}} + 0.05\right)^2 \times (t-t_0) + 1\right\}, \tag{12b}$$

where $t_{0,adj}$ is the modifying factor considering the effects of cement type and curing temperature to convert the age at loading t_0 to $t_{0,adj}$, which is equal to 8.03, 6.94

and 6.85 days for control, fly ash and GGBFS concrete, respectively, as shown in Eq. (12c):

$$t_{0,adj} = t_{0,T}\left[\frac{9}{2 + t_{0,T}^{1.2}} + 1\right]^{\alpha}, \tag{12c}$$

where α represents the coefficient ranging from − 1 to 1, depending on the type of cement, for example, − 1 for strength class 32.5 N, 0 for strength class 42.5 N and 1 for strength class 52.5 N, respectively (FIB, 2010). Moreover, (Dabarera et al., 2021) proved their model can work for different types of concrete (fly ash, silica fume concrete) without any adjustment. As a result, in this paper, the value of α is taken as 0 because the cement strength class of 42.5 is used. $t_{0,T}$ is the modified age at loading based on the curing history to take account into elevated or reduced temperatures on the maturity of concrete, as shown in Eq. (12d):

$$t_{0,T} = \sum_{i=1}^{n} \Delta t_i \exp\left[13.65 - \frac{4000}{273 + T(\Delta t_i)}\right], \tag{12d}$$

where Δt_i is the number of days where a temperature T occurs; $T(\Delta t_i)$ is the temperature in °C during the period of Δt_i.

Fig 11 presents the predicted basic tensile creep coefficient of all the concrete mixes. The start of calculation is assumed to be the same as autogenous shrinkage measurement (at 24 h after demoulding) due to the modelling purpose. The results stopped at the cracking when experimentally observed, i.e. 62, 104 and 92 h for control, fly ash and GGBFS concrete, respectively. It can be seen that the prediction results for fly ash concrete and GGBFS concrete were similar because of the similar temperature profile, while the reference concrete exhibited slightly lower results compared to that of SCMs-based concrete. This is attributed to a greater temperature profile due to a higher early age hydration degree, resulting in increased stiffness properties, leading to a decrease in creep (Briffaut et al., 2012). It indicated that the modified model suggested by (Dabarera et al., 2021) captured the evolution of the temperature profile and the basic tensile creep coefficient of concrete. In addition, a slightly lower tensile creep coefficient of control concrete contributed to a less stress relaxation to compensate for the tensile stress development, explaining a reduced cracking time of control concrete compared to that of fly ash and GGBFS concrete.

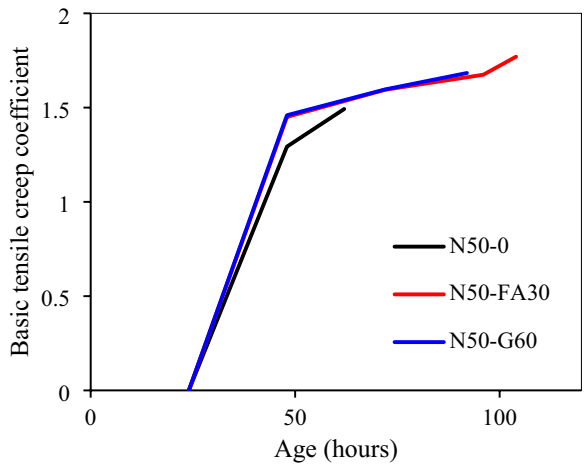

Fig. 11 Predictions of basic tensile creep coefficient using modified FIB, 2010 model

4.4 Comparison of Measured and Calculated Tensile Stress

Fig 12 shows the comparison of concrete tensile stress measured experimentally and tensile stress calculated analytically using Eq. (4). The experimental tensile stress can be computed using the measured Invar strain from strain gauges multiplied by the elastic modulus of Invar. The age-adjust effective modulus $\overline{E}_e$ can be calculated using the predicted values from the tensile creep coefficient model (see Fig. 11) and the time-dependent elastic modulus of concrete (Table 3). As such, D_R can be calculated using Eq. (5). The autogenous shrinkage-induced stress and thermally induced stress were calculated utilising Eqs. (9a) and (9b) are included for sensitivity analysis. It can be observed that the analytically calculated tensile stress as per Eq. (4) agrees well with experimentally measured tensile stress for all mixes, indicating the accurate prediction of the time-dependent tensile creep. The analytical maximum stress was also calculated using Eq. (1) to reveal the importance of tensile creep. The analytical maximum stress using Eq. (1) was greatly higher than experimental stress for all mixes, showing that the tensile creep can relax the concrete tensile stress and thus cannot be neglected. In addition, the thermal stress of reference concrete is much higher than that of fly ash and GGBFS concrete, leading to an accelerating cracking time.

4.5 Risk of Early Age Cracking

The risk coefficient is commonly used to assess the risk of early age concrete cracking (Khan et al., 2019a, 2019b, 2020). It is defined as the ratio between the concrete tensile stress calculated using Eq. (4) and the tensile strength of concrete, both being time-dependent, as shown in Eq. (13):

$$R(t) = \frac{\sigma_t(t)}{f_{ct}(t)}. \tag{13}$$

When the risk coefficient equals 0, there is no tensile stress developed in concrete, and the cracking does

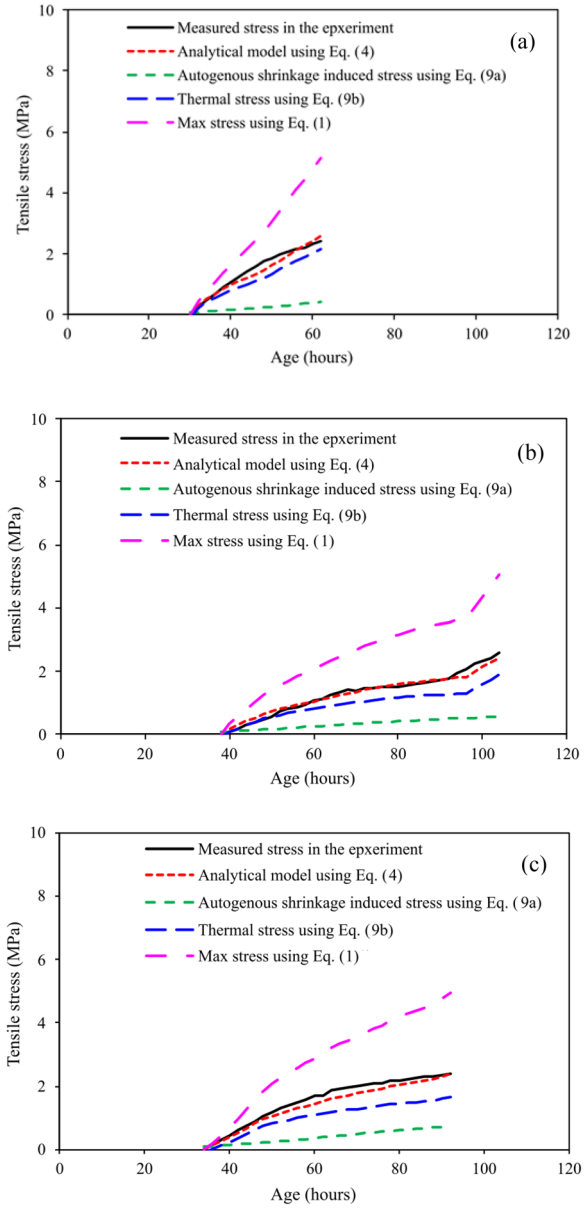

Fig. 12 Time-dependent stress development: **a** N50-0; **b** N50-FA30; **c** N50-G60

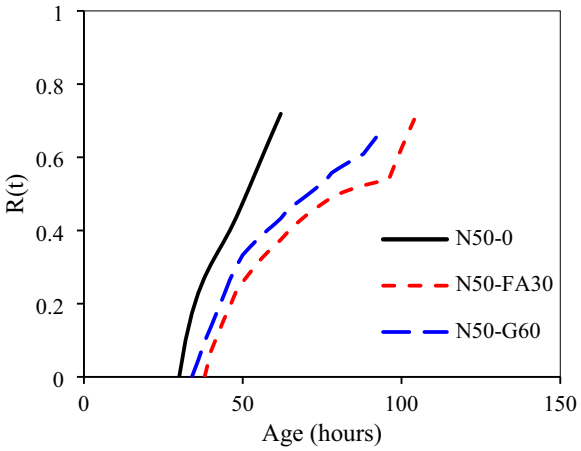

Fig. 13 Cracking risk coefficient R(t)

not occur. When the risk coefficient increases as tensile stress is generated gradually, the cracking risk becomes higher. Fig 13 shows the calculated cracking risk coefficient for the tested specimens until cracking occurs. It can be observed that at the same time, the $R(t)$ of N50-0 is the highest, followed by N50-G60, then N50-FA30. The calculated tensile stress of concrete at cracking is 72%, 70% and 65% of the splitting tensile strength for N50-0, N50-FA30 and N50-G60, respectively, which agrees with the results in (Altoubat & Lange, 2001; Khan et al., 2017). (Altoubat & Lange, 2001) reported that the cracking stress is taken to be 80% of direct tensile strength, and the direct tensile strength can be approximated as 80% of the splitting tensile strength for concrete at an age greater than 100 h. As such, the ratio of cracking stress to splitting tensile strength can be about 64%. (Khan et al., 2017) demonstrated that the cracking stress is equivalent to 65% of splitting tensile strength. Thus, these previous works supported the results of the calculated cracking risk coefficient of concrete in this research.

5 Summary and Conclusions

In this study, the early age cracking of concrete mixes with fly ash and GGBFS is experimentally investigated using the RCF. The free total deformations, including thermal strain and autogenous shrinkage, are measured by using the Free shrinkage frame (FSF). Mechanical properties are evaluated under match-curing conditions using an oven delivering the same temperature profile. The temperature profile was simulated using the software ConcreteWorks and applied to all relevant tests. The main observations are outlined below:

1. The free total deformation of control and SCMs mixtures exhibited an early age swelling. The control mixture showed higher swelling than SCMs concretes, which is attributed to the higher thermal dilatation. After the zero-stress time, the absolute free total deformation of the control concrete was higher than SCMs concrete, contributing to reduce the cracking time.
2. The time-dependent tensile strength and elastic modulus of fly ash and GGBFS concretes were lower than that of the control mixture under match-cur-

ing conditions, Similar trends were observed under standard curing or ambient curing conditions.

3. The predicted basic tensile creep coefficient of concrete mixes without SCMs was lower than with SCMs, leading to a lower early age stress relaxation. This was due to a greater temperature profile caused by a higher early age hydration degree, resulting in the increase of the stiffness properties, which led to a decrease in creep.
4. The risk of early age cracking of the reference concrete was the highest. This was mainly attributed to the higher free deformation due to a higher temperature rise. GGBFS concrete exhibited a higher autogenous shrinkage, leading to a shorter cracking time compared to fly ash concrete despite being exposed to a similar temperature profile. The concrete tensile stress at cracking was about 70% of the splitting tensile strength.
5. An analytical model was proposed to evaluate the early age tensile stress development due to restrained shrinkage and thermal expansion and contraction. This research can also contribute to developing a performance-based specification, allowing for avoiding experimentations using Rigid Cracking Frame (RCF) which are not straightforward tests.

Acknowledgements
This paper was funded by Cement Concrete Aggregates Australia and the Australian Research Council (Linkage Project LP170100912). The article processing charge was funded by Xihua University Project (Z231001). The author would like to thank the Centre for Infrastructure Engineering and Safety, School of Civil and Environmental Engineering, UNSW.

Author contributions
Yingda Zhang- writing-original draft, data curation, validation. Taehwan Kim- resources, validation, writing-review&editing, supervision. Arnaud Castel- methodology, supervision, project administration, writing review&editing. Tengfei Xu- supervision, writing review&editing.

Funding
This paper was funded by Cement Concrete Aggregates Australia and the Australian Research Council (Linkage Project LP170100912). The article processing charge was funded by Xihua University Project (Z231001).

Availability of data and materials
The data that support the findings of this study are available from the corresponding author upon reasonable request.

Declarations

Competing interests
The author declares no competing interests.

Received: 18 April 2023 Accepted: 22 July 2023
Published online: 11 December 2023

References

ACI207.1R-05. (2012). *Guide to mass concrete*. Farmington Hills: American Concrete Institute.
ACI207.2R-07. (2007). *Report on thermal and volume change effects on cracking of mass concrete*. Farmington Hills: American Concrete Institute.
ACI209R. (2008). *Prediction of creep, shrinkage, and temperature effects in concrete structures*. Farmington Hills: American Concrete Institute Committee 209.
Altoubat, S., & Lange, D. (2001). Creep, shrinkage, and cracking of restrained concrete at early age. *ACI Materials Journal, 98*(4), 323–331.
AS1012.10–2000. (2000). *Method of testing concrete—determination of indirect tensile strength of concrete cylinders (Brasil or splitting test)*. Sydney: Standard Australia.
AS1012.17–1997. (1997). *Method of testing concrete—determination of the static chord modulus of elasticity and Poisson's ratio of concrete specimens*. Sydney: Standard Australia.
AS1012.3.1–2014. (2014). *Methods of testing concrete—determination of properties related to the consistency of concrete—slump test*. Sydney: Standards Australia.
AS1012.4.2–2014. (2014). *Methods of testing concrete—determination of air content of freshly mixes concrete—measuring reduction in air pressure in chamber above concrete*. Sydney: Standards Australia.
AS1012.5–2014. (2014). *Methods of testing concrete—determination of mass per unit volume of freshly mixed concrete*. Sydney: Standard Australia.
AS1012.8.4–2015. (2015). *Methods of testing concrete—method for making and curing concrete—drying shrinkage specimens prepared in the field or in the laboratory*. Sydney: Standards Australia.
AS1012.9–2014. (2014). Methods of testing concrete - Compressive strength tests - Concrete, mortar and grout specimens. Australia.
AS2564–1982. (1982). *Aluminium ores—determination of aluminium, silicon, iron, titanium and phosphorus contents—wavelength dispersive X-ray fluorescence spectrometric method*. Sydney: Standard Australia.
AS3600–2018. (2018). *Australian standard for concrete structures*. Sydney: Standards Australia.
Atrushi, D. (2003). Tensile and compressive creep of early age concrete: Testing and modelling. The Norwegian University of Science and Technology, Norway: PhD Thesis.
Ballim, Y., & Graham, P. (2009). The effects of supplementary cementing materials in modifying the heat of hydration of concrete. *Materials and Structures, 42*(6), 803–811.
Batog, M., & Giergiczny, Z. (2017). Influence of mass concrete constituents on its properties. *Construction and Building Materials, 146*, 221–230.
Bissonnette, B., Pierre, P., & Pigeon, M. (1999). Influence of key parameters on drying shrinkage of cementitious materials. *Cement and Concrete Research, 29*(10), 1655–1662.
Bjøntegaard, Ø., Hammer, T., & Sellevold, E. (2004). On the measurement of free deformation of early age cement paste and concrete. *Cement and Concrete Composites, 26*(5), 427–435.
Breitenbucher, R. (1990). Investigation of thermal cracking with the cracking-frame. *Materials and Structures, 23*, 172–177.
Briffaut, M., Benboudjema, F., Torrenti, J., & Nahas, G. (2012). Concrete early age basic creep: experiments and test of rheological modelling approaches. *Construction and Building Materials, 36*, 373–380.
Byard, B., Schindler, A., Barnes, R., & Rao, A. (2010). Cracking tendency of bridge deck concrete. *Transportation Research Record, 2164*, 122–131.
Cai, C., Tang, H., Wen, T., Li, J., Chen, Z., Li, F., & Li, R. (2022). Long-term shrinkage performance and anti-cracking technology of concrete under dry-cold environment with large temperature differences. *Construction and Building Materials, 349*, 128730.
Carette, J., Joseph, S., Cizer, O., & Staquet, S. (2018). Decoupling the autogenous swelling from the self-desiccation deformation in early age concrete with mineral additions: micromacro observations and unified modelling. *Cement and Concrete Composites, 85*, 122–132.
Cheng, Z., Zhao, R., Yuan, Y., Li, F., Castel, A., & Xu, T. (2020). Ageing coefficient for early age tensile creep of blended slag and low calcium fly ash geopolymer concrete. *Construction and Building Materials, 262*, 119855.
Craeye, B., De Schutter, G., Desmet, B., Vantomme, J., Heirman, G., Vandewalle, L., & Kadri, E. (2010). Effect of mineral filler type on autogenous shrinkage of self-compacting concrete. *Cement and Concrete Research, 40*(6), 908–913.

Dabarera, A., Li, L., & Dao, V. (2021). Experimental evaluation and modelling of early-age basic tensile creep in high-performance concrete. *Materials and Structures, 54*(3), 130.
De Schutter, G., & Taerwe, L. (1996). Degree of hydration-based description of mechanical properties of early age concrete. *Materials and Structures, 29*(190), 335–344.
Eisa, M., Basiouny, M., & Fahmy, E. (2022). Drying shrinkage and thermal expansion of metakaolin-based geopolymer concrete pavement reinforced with biaxial geogrid. *Case Studies in Construction Materials, 17*, e01415.
FIB. (2010). *fib model code for concrete structures*. Wiley-VCH Verlag GmbH & Co. KGaA.
Gao, G., Qian, C., & Wang, Y. (2011). Effect of fly ash and slag powder on coefficient of thermal expansion of concrete. *Advanced Materials Research, 374–377*, 1230–1234.
Gao, Y., Zhang, H., Tang, S., & Liu, H. (2013). Study on early autogenous shrinkage and crack resistance of fly ash high-strength lightweight aggregate concrete. *Magazine of Concrete Research, 65*(15), 906–913.
Gibert, R., Castel, A., Khan, I., Mohammadi, J., South, W., & Thomas, T. (2017). Characterisation of autogenous shrinkage in Australian concrete. 28th Biennial Conference of the Concrete Institute of Australia. Adelaide: Concrete Institute of Australia.
Gilbert, R., & Ranzi, G. (2011). *Time-dependent behaviour of concrete structures*. Spon Press.
Gołaszewski, J., Klemczak, B., Golaszewska, M., Smolana, A., & Cygan, G. (2023). The feasibility of using a high volume of non-clinker binders in self-compacting concrete related to its basic engineering properties. *Journal of Building Engineering, 66*, 105893.
Gutsch, A. (2002). Properties of early age concrete—experiments and modelling. *Materials and Structures, 34*(246), 76–79.
Hansen, W., & Almndaiheem, J. (1987). Ultimate drying shrinkage of concrete—influence of major parameters. *ACI Materials Journal, 84*(3), 217–223.
Igarashi, S., Bentur, A., & Kovler, K. (2000). Autogenous shrinkage and induced restraining stresses in high-strength concretes. *Cement and Concrete Research, 30*(11), 1701–1707.
JCI. (2016). *Guidelines for control of cracking of mass concrete*. Tokyo: Japan Concrete Istitute.
Ji, G., Kanstad, T., Bjøntegaard, O., & Sellevold, E. (2013). Tensile and compressive creep deformations of hardening concrete containing mineral additives. *Materials and Structures, 46*(7), 1167–1182.
Khan, I., Castel, A., & Gilbert, R. (2017). Tensile creep and early-age concrete cracking due to restrained shrinkage. *Construction and Building Materials, 149*, 705–715.
Khan, I., Xu, T., Castel, A., & Gilbert, R. (2019a). Early-age tensile creep and shrinkage induced cracking in internally restrained concrete members. *Magazine of Concrete Research, 71*(22), 1167–1179.
Khan, I., Xu, T., Castel, A., Gilbert, R., & Babaee, M. (2019b). Risk of early age cracking in geopolymer concrete due to restrained shrinkage. *Construction and Building Materials, 229*, 116840.
Khan, I., Xu, T., Khan, M., Castel, A., & Gilbert, R. (2020). Effect of various supplementary cementitious materials on early-age concrete cracking. *Journal of Materials in Civil Engineering, 32*(4), 04020049.
Kovler, K. (1994). Testing system for determining the mechanical behaviour of early age concrete under restrained and free uniaxial shrinkage. *Materials and Structures, 27*, 324–330.
Kovler, K., & Zhutovsky, S. (2006). Overview and future trends of shrinkage research. *Materials and Structures, 39*(9), 827–847.
Lee, K., Lee, H., Lee, S., & Kim, G. (2006). Autogenous shrinkage of concrete containing granulated blast-furnace slag. *Cement and Concrete Research, 36*, 1279–1285.
Li, L., Dao, V., & Lura, P. (2021). Autogenous deformation and coefficient of thermal expansion of early-age concrete: initial outcomes of a study using a newly-developed temperature stress testing machine. *Cement and Concrete Composites, 119*, 103997.
Mangold, M. (1998). Prevention of Thermal Cracking in Concrete at Early Ages. London: Methods for Experimental Determination of Thermal Stresses and Crack Sensitivity in the Laboratory. In RILEM Report 15.
Markandeya, A., Shanahan, N., Gunatilake, D., Riding, K., & Zayed, A. (2018). Influence of slag composition on cracking potential of slag-Portland cement concrete. *Construction and Building Materials, 164*, 820–829.
Maruyama, I., & Lura, P. (2019). Properties of early-age concrete relevant to cracking in massive concrete. *Cement and Concrete Research, 105770*, 123.
Mehta, K., & Monteiro, P. (2006). *Concrete: microstructure, properties, and materials*. New York: McGraw-Hill Companies.
Neville, A., & Aitcin, P. (1998). High performance concrete—an overview. *Materials and Structures, 31*(2), 111–117.
Riding, K., Poole, J., Schindler, A., Juenger, M., & Folliard, K. (2008). Quantification of effects of fly ash type on concrete early-age cracking. *ACI Materials Journal, 105*(2), 149–155.
Sargam, Y., Faytarouni, M., Riding, K., Wang, K., Jahren, C., & Shen, J. (2019). Predicting thermal performance of a mass concrete foundation—a field monitoring case study. *Case Studies in Construction Materials, 11*, e00289.
Shui, Z., Zhang, R., Chen, W., & Xuan, D. (2010). Effects of mineral admixtures on the thermal expansion properties of hardened cement paste. *Construction and Building Materials, 24*, 1761–1767.
Slatnick, S., Riding, K., Folliard, K., Juenger, M., & Schindler, A. (2011). Evaluation of autogenous deformation of concrete at early ages. *ACI Materials Journal, 108*(1), 21–28.
Springenschmid, R., & Breitenbücher, R. (1998). *Influence of constituents, mix proportions and temperature on cracking sensitivity of concrete*. London: Prevention of Thermal Cracking in Concrete.
Springenschmid, R., Gierlinger, E., & Kiernozycki, W. (1985). *Thermal stresses in mass concrete: a new testing method and the influence of different cements*. Paris: 15th International Congress on Large Dams (ICOLD).
Tankasala, A., Schindler, A., & Riding, K. (2017). Risk of thermal cracking from use of lightweight aggregate in mass concrete. *Transportation Research Record, 2629*(1), 42–50.
Tao, Z., & Weizu, Q. (2006). Tensile creep due to restraining stresses in high-strength concrete at early ages. *Cement and Concrete Research, 36*(3), 584–591.
Truman, K., Petruska, D., & Norman, C. (1991). Creep, shrinkage, and thermal effects on mass concrete structure. *Journal of Engineering Mechanics, 117*(6), 1274–1288.
Wang, X., Xia, Q., & Zhu, P. (2015). Experimental research on the effect of ground slag on basic tensile creep of early-age concrete. *The Open Construction and Building Technology Journal, 9*(1), 68–72.
Wei, Y., & Hansen, W. (2013). Tensile creep behavior of concrete subject to constant restraint at very early ages. *Journal of Materials in Civil Engineering, 25*, 1277–1284.
Whigham, J. (2005). Evaluation of restraint stresses and cracking in early-age concrete with the rigid cracking frame. Auburn University: Master Thesis.
Zhang, Y., Afroz, S., Nguyen, Q., Kim, T., Castel, A., & Xu, T. (2022). Modeling blended cement concrete tensile creep for standard ring test application. *Structural Concrete*. https://doi.org/10.1002/suco.202200304
Zhang, Y., Afroz, S., Nguyen, Q., Kim, T., Eisentrager, J., Castel, A., & Xu, T. (2021). Analytical model predicting the concrete tensile stress development in the restrained shrinkage ring test. *Construction and Building Materials, 307*, 124930.
Zhu, B. (2014). *Thermal stresses & temperature control of mass concrete*. Beijing: Tsinghua University Press.

Publisher's Note

Yingda Zhang Assistant Professor and research secretary in the School of Architecture and Civil Engineering, Xihua University.